Chemical Engineering Journal 507 (2025) 160613

Contents lists available at ScienceDirect

Chemical Engineering Journal

journal homepage: www.elsevier.com/locate/cej

Ultrahigh energy density in high-temperature polymer dielectric reinforced by bilayer nanocoating

Yifei Wang [a,b,*], Thomas Linker [c], K.M. Abu Hurayra Lizu [d], Luis A. Ortiz-Flores [d], Deepak Kamal [e], Jierui Zhou [b], Hiep Nguyen [b], Chuanyang Li [b], Wenqiang Gao [b,f], Antigoni Konstantinou [b], Lihua Chen [e], Bryan D. Huey [d], Rampi Ramprasad [e], Aiichiro Nakano [c], Fuyuki Shimojo [g], Priya Vashishta [c], Yang Cao [b,f,*]

[a] State Key Laboratory for Mechanical Behavior of Materials, School of Materials Science and Engineering, Xi'an Jiaotong University, Xi'an, PR China
[b] Electrical Insulation Research Center, Institute of Materials Science, University of Connecticut, Storrs, CT 06269, USA
[c] Collaboratory for Advanced Computing and Simulations, University of Southern California, Los Angeles, CA 90089-0242, USA
[d] Department of Materials Science and Engineering, University of Connecticut, Storrs, CT 06269, USA
[e] School of Materials Science and Engineering, Georgia Institute of Technology, Atlanta, GA 30332, USA
[f] Department of Electrical and Computer Engineering, University of Connecticut, Storrs, CT 06269, USA
[g] Department of Physics, Kumamoto University, Kumamoto 860-8555, Japan

ARTICLE INFO

Keywords:
Dielectric energy storage
Nanocoating
Electrical insulation
Interface engineering

ABSTRACT

Next-generation electrical and power electronic systems necessitate polymer dielectrics with high energy densities and high-temperature applicability. However, such ever-increasing performance demands result in exponential increases of leakage electrical conduction, which is fundamentally associated with thermally and electrically assisted charge injection and transport mechanisms. Here, we report a substantial improvement in high-temperature energy storage properties for polymer dielectrics with a bilayer nanocoating. Two-dimensional boron nitride and montmorillonite nanosheets were coated on the polymer surface, showing a synergetic effect on trapping and dissipating the hot carriers injected from electrodes. We obtain an ultrahigh discharged energy density of 5.5 J/cm^3 with an efficiency exceeding 90 % at 150 °C. This bilayer nanocoating strategy provides a generalizable approach for designing high-performance polymer dielectrics via interfacial engineering.

1. Introduction

Electrostatic capacitors are critical components in electrical and power electronic systems owing to their fast charge–discharge capability for high-power electrical energy storage [1–3]. Polymer dielectrics are preferred materials for electrostatic capacitors because of their high breakdown strength, flexibility, reliability, low cost, and lightweight [4–9]. However, the implementation of polymer dielectrics in high-voltage capacitors at high operation temperatures is still a bottleneck [10]. For example, biaxially oriented polypropylene (BOPP), as the state-of-the-art commercially available polymer dielectric, can only operate at a temperature lower than 105 °C [11,12]. To meet the requirement of harsh operating conditions and increased energy levels for future electrical energy storage needs, high-temperature polymer dielectrics with high energy densities are therefore of both fundamental and applied interest [13–15]. Although many engineered polymers with high glass transition temperatures have been developed, they all suffer undesirably increased conduction losses at elevated electric fields and temperatures [16–19]. This leads to not only low dischargeable energy density but also severe thermal runaway which raises great challenges for long-term reliability of capacitors operating under extreme conditions.

After years of effort, it has been realized that the sharply increased charge injection at high temperatures is one of the main causes of high conduction loss. The surge in kinetic energy of charge carriers endows them with the ability to cross the electrode-dielectric interface barrier [20,21]. One common approach for addressing this problem is to add an inorganic coating layer with a large bandgap on the polymer surface to further enhance the interface barrier height [22,23]. However, the resulting blocked charges at the interface will accumulate, leading to an

* Corresponding authors.
E-mail addresses: yifei.wang@xjtu.edu.cn (Y. Wang), yang.cao@uconn.edu (Y. Cao).

https://doi.org/10.1016/j.cej.2025.160613
Received 8 October 2024; Received in revised form 6 December 2024; Accepted 11 February 2025
Available online 13 February 2025

increase in the local electric field strength and thus the generation of surface defects. Correspondingly, it is still difficult for polymer dielectrics to obtain high charge–discharge efficiency (> 90 %) and high energy storage density (> 4 J/cm^3) under high temperatures (150 °C) and high electric fields (500 MV/m).

Here, we present a bilayer nanocoating structure, which introduces a charge dissipation coating layer between a large-bandgap coating layer and the underlying polymer dielectric. The modulation mechanism of the bilayer nanocoating on the charge injection is shown in Fig. 1: firstly, injected charge is trapped in the outer coating, and then the inner coating dissipates the captured charge along the interface. In our approach, the charge dissipation layer comprises montmorillonite (MMT) nanosheets. MMT has a larger through-thickness bandgap and a relatively high in-plane electrical conductivity [24]. This electrical anisotropy not only achieves the desired charge dissipation along the interface to avoid penetrating into the polymer dielectric, but also solves the problem of surface charge accumulation, thereby effectively alleviating the local electric field strength.

2. Methods

2.1. Materials

To make the polymer film, soluble polycarbonate (PC) pellets (PolyK) were first dissolved in chloroform and cast onto a glass substrate. The cast films were dried at 100 °C and then peeled off from the substrate in water. The free-standing films were obtained by finally drying at 130 °C to remove all residual solvent and water. To perform nanocoating on a polymer substrate, MMT and boron nitride (BN) coating precursors were prepared in advance. MMT and BN nanosheets were exfoliated in ethanol via tip sonication (100 w, 1 h), respectively. Polyvinyl butyral (PVB) powders were then dissolved into the above suspension by magnetic stirring. After the PVB was completely dissolved, the solutions were tip-sonicated for 1 h again to ensure the uniform dispersion of the nanosheets. The bilayer nanocoatings were manufactured by a two-step dip coating method. Taking BN-MMT-PC as an example, the PC film was first dipped into the MMT coating precursor. After standing for 30 s, the film was slowly lifted and dried at 30 °C for 5 min. This process was followed by a second-round dip coating with the BN coating precursor. Finally, the coated PC film was completely dried at 100 °C overnight. The manufacturing of single-material-coated PC follows the same process while using only one material (either BN or MMT) coating precursor two times. This can make sure all the coated films have the same coating thickness.

2.2. Morphology and structure Characterization

The morphology of the coated films was characterized by scanning electron microscopy (SEM, FEI Teneo Verios). To elucidate the layer-by-layer distribution of the BN and MMT nanocoatings on the thin film substrates, the grazing incident X-ray diffraction (GIXRD) technique was implemented by using a Rigaku SmartLab X-ray diffractometer. The instrument is equipped with a 9 kW copper rotating anode to generate high-intensity X-ray flux and a HyPix-3000 1D/2D detector for fast signal collection. During measurements, the incident angle of the X-ray source is set fixed while the detector arm rotates to collect the data. The higher the incident angle is, the deeper the X-ray goes through the sample surface. Therefore, the GIXRD diffraction pattern provides depth-dependent crystallography and thus the distribution of the nanoparticle layers. The X-ray incident angle was chosen from 0.1° to 5.0°.

2.3. Thermal Analysis

A TA Instruments Q-100 was used for differential scanning calorimetry (DSC) measurements, with a temperature ramping rate of 10 °C/min.

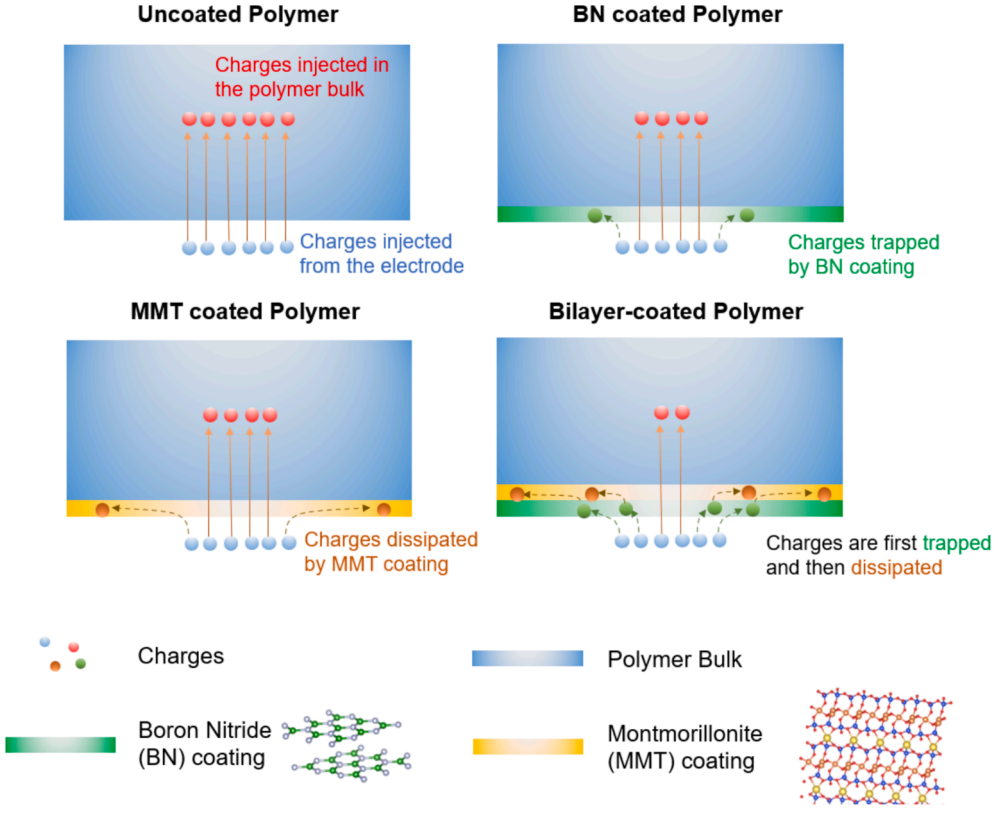

Fig. 1. Schematic illustration of bilayer coating. The injected charges will be trapped by BN first and then dissipated in the MMT coating layer.

2.4. Electrical Characterization

A resistor–capacitor circuit with a linear voltage ramp of 300 V/s was used to measure dielectric breakdown strength. When the breakdown happens, an interlock input can be used to turn the power supply off. A peak-holding voltmeter was used to measure the breakdown voltage. A pair of needle-to-plate electrodes were used for the surface potential decay test, with the sample placed on the plate electrode 6 mm away from the needle electrode. A DC voltage of 6 kV was applied to the needle for 1 min to perform the corona charge, then the sample was transferred under a probe for 2 min to monitor the surface potential decay. For other electrical measurements, gold/palladium electrodes were sputtered on all the samples (6002–8 Ted Pella, Inc.). An impedance analyzer (Solartron 1260) and a resistance meter were used to obtain dielectric spectra over a wide temperature range. A modified Sawyer-Tower circuit was used to measure the high-field electric displacement-electric field (*D-E*) loops at 100 Hz. A lab-designed capacitive cancellation measurement system was used to measure pre-breakdown conduction at elevated temperatures [31]. A dynamic gain-controlled negative feedback loop successfully cancels the capacitive current, and the signal output reflects the time-integrated conduction current.

2.5. Kelvin Probe Force Microscopy (KPFM) Measurements

A dual-pass procedure is employed with a commercial AFM (Asylum Research, Cypher ES), where surface topography is obtained by regular AC mode imaging, followed by non-contact scanning with a fixed tip-sample separation (nominally 50 nm). This essentially establishes a nano-capacitor between the surface and the AFM probe (ASYLEC-01-R2, Oxford Instruments), which is biased with an AC voltage driving the cantilever at resonance for optimal sensitivity to electrical forces acting between the tip and sample. A feedback loop then continuously updates a superimposed DC voltage to null these tip-sample interactions, a condition that is only met when the tip bias equilibrates the effective potential at the surface below and thereby can be used for mapping. Here, following an initial charging step employing negative 6 V over a small central 100 nm × 50 nm region, tens of larger area KPFM scans are acquired continuously to record the charge distribution and its evolution with time. Analyzing the exponential decay pixel by pixel allows the charge dissipation behavior to be assessed and mapped [32]. It is noteworthy that the initial charge distribution (first image in each example) is seldom uniform, and that the differences between all following images and the first image are therefore always utilized for any further analysis.

2.6. Non-Adiabatic Quantum Molecular Dynamics (NAQMD) Simulations

NAQMD simulation is performed in the framework time-dependent density functional theory (TDDFT) with excited state forces computed on atoms and phonon-assisted exciting transitions between electronic states modeled within the surface hopping approach [33–36]. Energies and forces were computed using a plane wave basis within the projected augmented wave-vector (PAW) method [37]. Projector functions were generated for the 1 s hydrogen, 2 s and 2p carbon, 2 s and 2p boron, 2 s and 2p nitrogen, 3 s, 3p, 3d sodium, 2 s, and 2p oxygen, 3 s, 3p and 3d Al states, and 3 s, 3p and 3d Si states. A plane-wave cutoff of 35ry and 300ry were used for the wave functions and density respectively. The gamma point was used to sample the Birullion zone. The Perdew–Burke–Ernzerhof (PBE) styled generalized gradient approximation (GGA) for the exchange–correlation functional was used, and Van der Walls interactions were included with the DFT-D method [38,39]. All calculations were performed in the QXMD software.

NAQMD for the BN-PC structure was performed on an interface created in the (110) plane. The interface consisted of 1 × 2 × 2 2-chain unit cells of PC sandwiched, (with the chain direction along [001] axis), between two separate 240-atom bilayers of BN. An additional 17Å of vacuum was provided to the surface, and the electric field was modeled with a sawtooth potential. The PC crystal structure was created by the reference from the Khazana database. Of these candidate structures, the lowest PBE-DFT energy PC crystal structure that was non-polar was then used for NAQMD simulation. NAQMD simulation was performed with a time-step of 0.216 fs, within the NVT ensemble [40].

NAQMD for the MMT crystal was performed on orthorhombic supercells containing three MMT nanosheets with an open surface, and periodic boundary conditions(PBC). The PBC supercell dimensions were 5.25Å × 9.14Å × 31.46 Å and 5.25Å × 9.14Å × 50.0 Å for the surface system to remove image interactions along the thickness direction. NAQMD simulation was performed with a time-step of 1.216 fs, within the NVT ensemble.

To quantify the energy loss rate k, we calculated the average electronic excitation energy as a function of time,

$$Eexc(t) = \frac{\sum_i f_i(t)\epsilon_i(t)\theta(\epsilon_i(t)) - \sum_i (1 - f_i(t))\epsilon_i(t)\theta(-\epsilon_i(t))}{\sum_i f_i(t)\epsilon_i(t)\theta(\epsilon_i(t)) + \sum_i (1 - f_i(t))\epsilon_i(t)\theta(-\epsilon_i(t))}$$

where $f_i(t)$ is the occupation of the i^{th} band at time t, $\epsilon_i(t)$ is the KS energy, and θ is the heavy-side function. The rate k was determined by a semi-log fit of the excitation energy as a function of time over the exponential decay period of the energy.

3. Results and Discussion

We investigate the efficacy of such a BN/MMT bilayer nanocoating, deposited on a solution-cast polycarbonate (PC) film via dip-coating, considering both possible layer sequences (BN-MMT-PC and MMT-BN-PC). Polymers with single material coatings and uncoated film were also prepared for controls (BN-PC, MMT-PC, and PC). The morphology and structures of each specimen were analyzed by SEM and GIXRD (Supplementary Fig. S1-2). The large-scale charge dynamics were examined by a macroscopic surface potential decay measurement on coated polymer films with an area of 5 × 5 cm^2 (Fig. 2a). After corona charging by a high voltage of 6 kV for 1 min, compared with uncoated PC, BN-PC shows a high initial surface potential and a long retention time. Conversely, the charge dissipation for a pure MMT coating is rapid, and the much reduced initial surface potential indicates most injected charges are dissipated even before the first measurements can be made (after a necessary delay while switching from charging to detection modes). As proposed, the bilayer-coated film simultaneously inherits the benefits of BN and MMT coatings. That is, charges trapped by the BN layer endow BN-MMT-PC with a comparable initial surface potential as that of uncoated PC, but it rapidly decays due to effective charge dissipation by the interposing MMT coating. Finally, when we reverse the order of the BN and MMT coatings, a lower initial surface potential is observed as anticipated for MMT-BN-PC. The outside MMT dissipates charges more effectively, though the underlying BN can still trap penetrated charges and result in a higher surface potential, compared with only MMT-PC.

Such charge dynamics are confirmed at the microscale for the variously coated polymers using KPFM, as shown in Fig. 2b. The sample surface is charged by applying a negative DC bias of −6 V during point contact in the center of the field of view. As demonstrated in the potential profiles of Fig. S4, for BN-MMT-PC, the external BN coating effectively traps charge, evidenced by a pronounced central surface potential peak and slow potential decay. As can be seen, it takes approximately 500 s for the surface potential to diminish by only ~ 100 mV. On the contrary, surface potential maps following identical biasing for MMT-BN-PC (profiles in Fig. S5) demonstrate a nearly immediate decay of the initially charged surface, enabled by in-plane charge spreading via the external MMT coating. As a control, Fig. S6 presents charging and decay for just BN-PC, with anticipated slow charge decay.

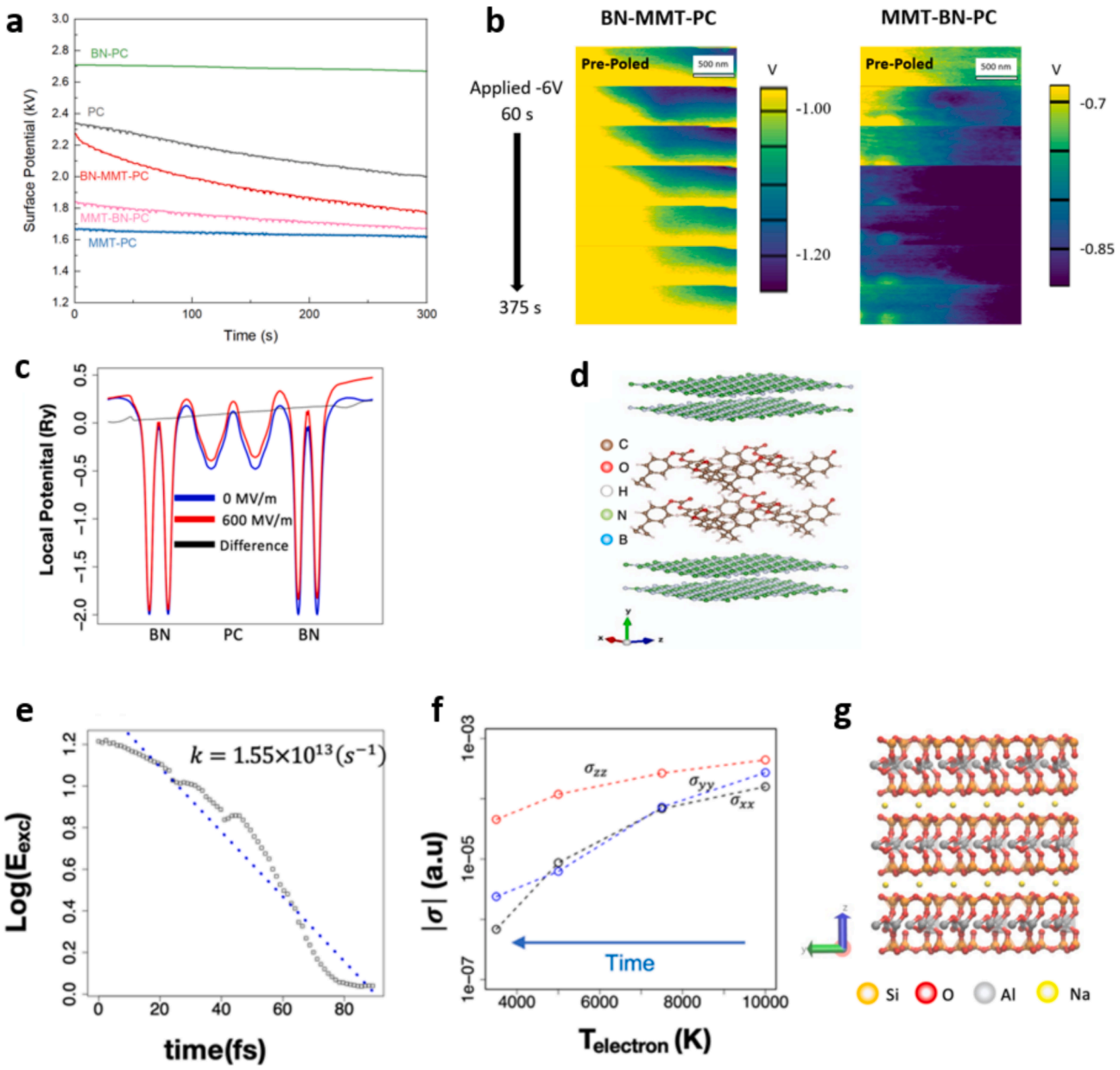

Fig. 2. Hot Carrier Dynamics. a. surface potential decay. BN nanocoating traps charges with high surface potential, while MMT can dissipate charges, thus showing suppressed surface potential. **b.** KPFM surface charge dissipation. Central charge spots were "poled" with −6 V on the surface of BN-MMT-PC and MMT-BN-PC. **c.** Calculated local potential profile for BN-PC interface. Deep well potential was found to trap hot carriers in NAQMD simulation. **d.** Molecular model of Bn-PC interface. **e.** Rapid energy dissipation of hot carrier energy in MMT surface under electric field. **f.** Dynamic Decay of Conductivity as a function of effective electron temperature indicates more rapid decay of the carrier conduction in a plane versus along the Vander-Waals/thickness direction. **g.** Molecular model of MMT.

We further investigate the charge dynamics in the polymer dielectric with nanocoatings of BN and MMT using a NAQMD simulation. We considered a PC-BN layer structure as depicted in Fig. 2c-d. A sawtooth potential was applied along the vacuum direction to simulate the presence of an electric field. The local potential profile under the influence of the applied field demonstrates a deep-potential well formed in the BN layers, indicating the ability of BN to trap hot carriers. During the NAQMD simulation, a slow carrier relaxation process was observed with a computed relaxation rate of $k = 1.3 \times 10^{12}$ (s^{-1}) (Supplementary Fig. S8). To evaluate the MMT nanocoating, we performed NAQMD simulations on the surface and bulk supercell containing three MMT nanosheets (see methods for details), which is imaged in Fig. 2e. The simulation was performed under an electric field on the surface supercell with hot electron-hole pair generated from deep within the valence band. A rapid dissipation (~80 fs) of the carrier energy was observed, with an order of magnitude increase of the computed rate in comparison to BN ($k = 1.6 \times 10^{13}$). To further evaluate hot carrier dynamics in MMT, we performed NAQMD simulations on a bulk supercell where we found anisotropies in the hole and electron mobility (Supplementary Fig. S11), with a much higher electron than hole mobility after the initial carrier relaxation. Carriers were found to be delocalized in the *xy* plane while more localized to an individual nano-sheet (*z* axis), indicating higher in-plane mobility of carriers versus along the Vander-walls bonded direction of the 2D nano-sheet. To understand the directional dependance of carrier dissipation, we computed the conductivity through the Green-Kubo Formula as a function of electronic temperature which is illustrated in Fig. 2f. As carrier energy is dissipated through electron–phonon scattering, their effective electronic temperature will decline, which can be modeled using an electronic temperature that is out of equilibrium with the lattice temperature. Fig. 2f illustrates a much

more rapid decay as a function of the decreasing electronic temperature in the conductivity in the *xy* plane versus along the Vander-Waals/thickness direction (*z* axis), indicating more efficient dissipation of the carrier energy transversely. Overall, the simulation results indicate that BN will be an effective coat for trapping hot carriers, whereas MMT will effectively dissipate carrier energies, with primary dissipation being in a plane versus along the Vander-Waals direction.

We proceed to examine the high-field conduction by measuring leakage current density (Fig. 3a). Either BN or MMT coating can reduce the current density, indicating the conduction can be effectively suppressed by (1) blocking the charge injection or (2) dissipating the injected charges. The synergetic effect of BN and MMT coatings is well shown in the BN-MMT-PC, which possesses the lowest leakage current among all coated films. It should be noticed that the conduction in MMT-BN-PC is relatively high, meaning the sequence of the coating materials is significant. We assume BN coating with charge-trapping capability should be placed near the electrode and thus efficiently reduce the number of charges that could penetrate through the outside coating. Then, those charges that can still be injected can be dissipated in the MMT coating that is positioned between the BN coating and polymers. However, in the case of MMT-BN-PC, injected charges hold a greater chance to penetrate through the outside MMT layer. They are accelerated by the applied electric field, which makes them hard to be captured in the inside BN coating, eventually causing a higher leakage current.

We then studied the dielectric properties with the measurement of temperature-dependent dielectric spectrum (Supplementary Fig. S12). The nanocoatings show little influence on the dielectric constant, which is ~ 3 at 1 kHz and 150 ℃ in all coated and uncoated PC (Fig. 3b). Attributed by the suppressed conduction, BN-MMT-PC shows the lowest dielectric loss, suggesting enhanced energy storage properties at high temperature. The high-temperature insulating properties were then testified by breakdown measurement at 150 ℃. More than ten films of each sample were tested to failed to obtain the Weibull statistical values of breakdown strength (Fig. 3c and Fig. S13). The breakdown strength of PC is enhanced via performing surface coating, especially with bilayer nanocoating. For example, BN-MMT-PC has the highest breakdown strength of 620 MV/m, which is 20 % higher than the uncoated PC. It should be noticed that this BN-MMT coating also improves the film uniformity and quality, as reflected by a much improved shape factor (from 7 to 20).

To obtain high-temperature capacitive energy storage performance, we measured bipolar electric displacement-electric field (*D-E*) hysteresis loops at 150 °C. Attributed to the enhanced breakdown strength, a high discharged energy density of 7 J/cm^3 is achieved in BN-MMT-PC, which is 50% higher than that in uncoated PC. As the bilayer coating dramatically suppresses high-field conduction, an improved charge–discharge efficiency is also achieved in BN-MMT-PC. For example, the efficiency drops below 90% in uncoated PC at 200 MV/m, while BN-MMT-PC can maintain a high efficiency (>90%) even at an electric field higher than 500 MV/m. Consequently, the energy density at an efficiency higher than 90 % increases from 1 J/cm^3 in uncoated PC to 5 J/cm^3 in BN-MMT bilayer-coated PC. We compared the energy storage performance of BN-MMT-PC with the state-of-the-art high-temperature polymer-based dielectrics, as summarized in Fig. 4d [7,25–30]. No previously reported dielectrics can deliver an energy density exceeding 3.5 J/cm^3 with an efficiency higher than 90% at 150 °C. This upper limit

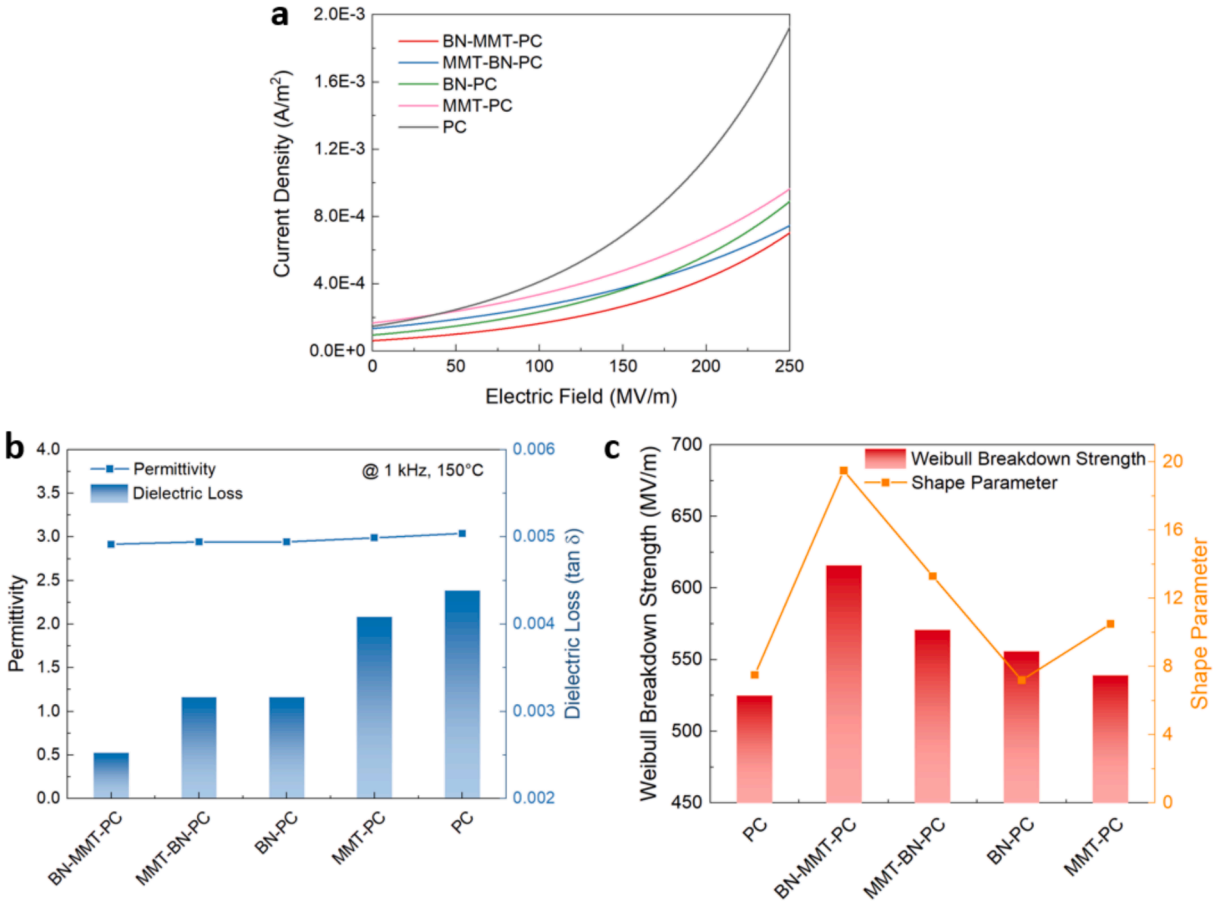

Fig. 3. Electrical insulation and dielectric properties of bilayer-coated PC. a. leakage current density. Due to the synergetic effect of BN and MMT coating, bilayer-coated PC shows the lowest current density. **b.** permittivity and dielectric loss. As a result of the suppressed conduction, BN-MMT bilayer-coated PC shows the lowest dielectric loss. **c.** breakdown strength. The bilayer coating endows the PC with enhanced breakdown strength and improves the homogeneity of the PC, as evidenced by the higher shape parameter.

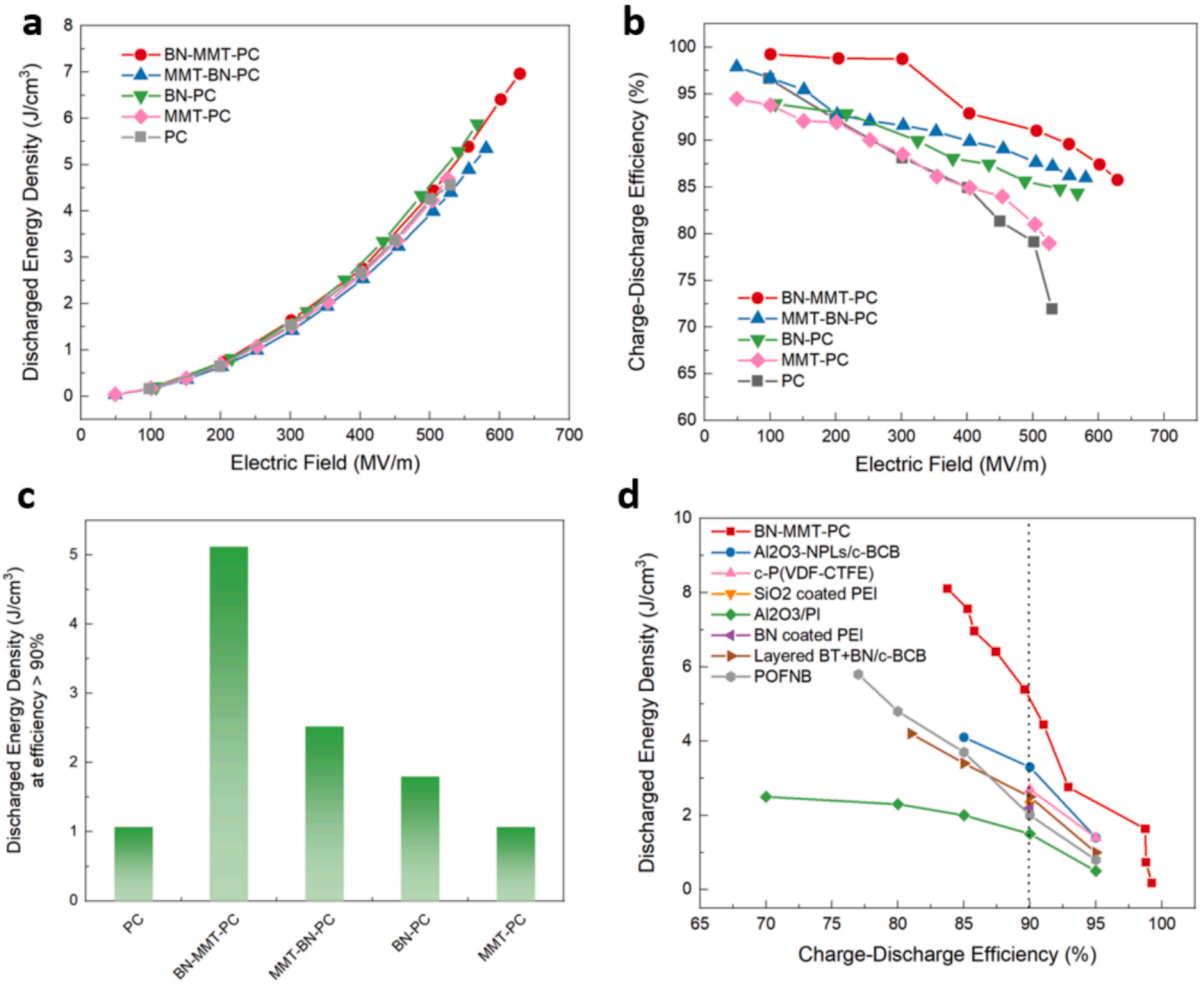

Fig. 4. High-temperature (150°C) energy storage properties of bilayer-coated PC. a. discharged energy density, **b.** charge–discharge efficiency, **c.** energy density at an efficiency higher than 90 %, and **d.** comparison of the bilayer-coated PC with previously reported polymer dielectrics. The BN-MMT bilayer coating can enhance efficiency due to its charge blocking and dissipating effect. The energy density can be improved from 1 J/cm^3 to 5.5 J/cm^3 with the bilayer coating at 150°C. Compared with other polymer dielectrics, our bilayer coated PC shows the highest energy density at the same efficiency.

is raised by around 50% in our work (5.5 J/cm^3). The superiority of our novel bilayer-coated film is even further enhanced for charge–discharge efficiencies of 80%.

4. Conclusion

In summary, we have elevated high-temperature capacitive performance in the bilayer-coated polymer at elevated temperatures. This distinctive feature originates from the synergistic effect of charge trapping (BN) and charge dissipation (MMT) that effectively suppress charge injection and thus leakage conduction loss. Crucially, the solution-based cast and dip coating fabrication is scalable for large-area roll-to-roll processing. Our findings establish bilayer coating with a sequence of 2D materials arrangement as a promising (external BN plus internal MMT) design platform to engineering dielectric surfaces for next-generation capacitive energy storage.

CRediT authorship contribution statement

Yifei Wang: Writing – review & editing, Writing – original draft, Methodology, Investigation, Formal analysis, Data curation, Conceptualization. **Thomas Linker:** Writing – review & editing, Investigation. **K. M. Abu Hurayra Lizu:** Data curation. **Luis A. Ortiz-Flores:** Formal analysis. **Deepak Kamal:** Data curation. **Jierui Zhou:** Validation. **Hiep Nguyen:** Visualization. **Chuanyang Li:** Validation. **Wenqiang Gao:** Validation. **Antigoni Konstantinou:** Validation. **Lihua Chen:** Visualization. **Bryan D. Huey:** Writing – review & editing, Supervision. **Rampi Ramprasad:** Supervision, Software, Resources. **Aiichiro Nakano:** Writing – review & editing, Supervision. **Fuyuki Shimojo:** Validation. **Priya Vashishta:** Supervision, Software, Resources. **Yang Cao:** Writing – review & editing, Supervision, Resources, Project administration.

Declaration of competing interest

The authors declare that they have no known competing financial interests or personal relationships that could have appeared to influence the work reported in this paper.

Acknowledgements

This work was supported through a multidisciplinary university research initiative (MURI) grant (N00014-17-1-2656) and a capacitor program grant (N0014-19-1-2340), both from ONR.

Appendix A. Supplementary data

Supplementary data to this article can be found online at https://doi.org/10.1016/j.cej.2025.160613.

Data availability

Data will be made available on request.

References

[1] J. Chen, et al., Ladderphane copolymers for high-temperature capacitive energy storage, *Nature* 615 (2023) 62–66.
[2] W. Sarjeant, I.W. Clelland, R.A. Price, Capacitive components for power electronics, *Proc. IEEE* 89 (2001) 846–855.
[3] S. Luo, et al., Construction of a 3D-BaTiO3 network leading to significantly enhanced dielectric permittivity and energy storage density of polymer composites, *Energy Environ. Sci.* 10 (2017) 137–144.
[4] B. Chu, et al., A dielectric polymer with high electric energy density and fast discharge speed, *Science* 313 (2006) 334–336.
[5] Q. Li, et al., Flexible high-temperature dielectric materials from polymer nanocomposites, *Nature* 523 (2015) 576–579.
[6] H. Li, et al., Dielectric polymers for high-temperature capacitive energy storage, *Chem. Soc. Rev.* 50 (2021) 6369–6400.
[7] C. Wu, et al., Flexible Temperature-Invariant Polymer Dielectrics with Large Bandgap, *Adv. Mater.* 32 (2020) e2000499.
[8] J.S. Ho, S.G. Greenbaum, Polymer Capacitor Dielectrics for High Temperature Applications, *ACS Appl. Mater. Interfaces* 10 (2018) 29189–29218.
[9] T. Zhang, et al., Recent progress in polymer dielectric energy storage: From film fabrication and modification to capacitor performance and application, *Prog. Mater Sci.* 140 (2023).
[10] D. Tan, L. Zhang, Q. Chen, P. Irwin, High-temperature capacitor polymer films, *J. Electron. Mater.* 43 (2014) 4569–4575.
[11] Z. Zhang, D.H. Wang, M.H. Litt, L.S. Tan, L. Zhu, High-Temperature and High-Energy-Density Dipolar Glass Polymers Based on Sulfonylated Poly(2,6-dimethyl-1,4-phenylene oxide), *Angew. Chem. Int. Ed. Engl.* 57 (2018) 1528–1531.
[12] M. Rabuffi, G. Picci, Status quo and future prospects for metallized polypropylene energy storage capacitors, *IEEE Trans. Plasma Sci.* 30 (2002) 1939–1942.
[13] T. Zhang, et al., A highly scalable dielectric metamaterial with superior capacitor performance over a broad temperature, *Sci. Adv.* 6 (2020) eaax6622.
[14] Z. Pan, et al., Tailoring Poly(Styrene-co-maleic anhydride) Networks for All-Polymer Dielectrics Exhibiting Ultrahigh Energy Density and Charge-Discharge Efficiency at Elevated Temperatures, *Adv. Mater.* 35 (2023) e2207580.
[15] M. Yang, W. Ren, M. Guo, Y. Shen, High-Energy-Density and High Efficiency Polymer Dielectrics for High Temperature Electrostatic Energy Storage: A Review, *Small* 18 (2022) e2205247.
[16] Q. Li, et al., High-Temperature Dielectric Materials for Electrical Energy Storage, *Ann. Rev. Mater. Res.* 48 (2018) 219–243.
[17] X. Li, et al., Unraveling bilayer interfacial features and their effects in polar polymer nanocomposites, *Nat Commun* 14 (2023) 5707.
[18] Y. Zhu, et al., High Conduction Band Inorganic Layers for Distinct Enhancement of Electrical Energy Storage in Polymer Nanocomposites, *Nanomicro Lett* 14 (2022) 151.
[19] J. Zhou, et al., High-temperature dielectric energy storage films with self-co-assembled hot-electron blocking nanocoatings, *Nano Energy* 120 (2024) 109184.
[20] Y. Wang, et al., Sandwiched Polymer Nanocomposites Reinforced by Two-Dimensional Interface Nanocoating for Ultrahigh Energy Storage Performance at Elevated Temperatures, *Small* 19 (2023) e2208105.
[21] H. Luo, et al., Interface design for high energy density polymer nanocomposites, *Chem. Soc. Rev.* 48 (2019) 4424–4465.
[22] P. Wang, et al., Ultrahigh Energy Storage Performance of Layered Polymer Nanocomposites over a Broad Temperature Range, *Adv. Mater.* 33 (2021) e2103338.
[23] Y. Wang, et al., Tuning Surface States of Metal/Polymer Contacts Toward Highly Insulating Polymer-Based Dielectrics, *ACS Appl. Mater. Interfaces* 13 (2021) 46142–46150.
[24] Y. Wang, et al., Interfacial 2D Montmorillonite Nanocoatings Enable Sandwiched Polymer Nanocomposites to Exhibit Ultrahigh Capacitive Energy Storage Performance at Elevated Temperatures, *Adv Sci (weinh)* 9 (2022) e2204760.
[25] H. Li, et al., Scalable Polymer Nanocomposites with Record High-Temperature Capacitive Performance Enabled by Rationally Designed Nanostructured Inorganic Fillers, *Adv. Mater.* 31 (2019) e1900875.
[26] H. Li, et al., Crosslinked fluoropolymers exhibiting superior high-temperature energy density and charge–discharge efficiency, *Energy Environ. Sci.* 13 (2020) 1279–1286.
[27] Y. Zhou, et al., A Scalable, High-Throughput, and Environmentally Benign Approach to Polymer Dielectrics Exhibiting Significantly Improved Capacitive Performance at High Temperatures, *Adv. Mater.* 30 (2018) 1805672.
[28] D. Ai, et al., Tuning Nanofillers in In Situ Prepared Polyimide Nanocomposites for High-Temperature Capacitive Energy Storage, *Adv. Energy Mater.* 10 (2020) 1903881.
[29] A. Azizi, et al., High-Performance Polymers Sandwiched with Chemical Vapor Deposited Hexagonal Boron Nitrides as Scalable High-Temperature Dielectric Materials, *Adv. Mater.* 29 (2017) 1701864.
[30] Q. Li, et al., Sandwich-structured polymer nanocomposites with high energy density and great charge-discharge efficiency at elevated temperatures, *Proc. Natl. Acad. Sci. u.s.a.* 113 (2016) 9995–10000.
[31] Z. Li, C. Xu, H. Uehara, S. Boggs, Y. Cao, Transient characterization of extreme field conduction in dielectrics, *AIP Adv.* 6 (2016) 115025.
[32] T.J. Moran, K. Suzuki, T. Hosokura, A. Khaetskii, B.D. Huey, Charge injection and decay of nanoscale dielectric films resolved via dynamic scanning probe microscopy, *J. Am. Ceram. Soc.* 104 (2021) 5157–5167.
[33] C.F. Craig, W.R. Duncan, O.V. Prezhdo, Trajectory surface hopping in the time-dependent Kohn-Sham approach for electron-nuclear dynamics, *Phys. Rev. Lett.* 95 (2005) 163001.
[34] E. Runge, E.K. Gross, Density-functional theory for time-dependent systems, *Phys. Rev. Lett.* 52 (1984) 997.
[35] F. Shimojo, et al., A divide-conquer-recombine algorithmic paradigm for large spatiotemporal quantum molecular dynamics simulations, *J. Chem. Phys.* 140 (2014) 18A529.
[36] J.C. Tully, Molecular dynamics with electronic transitions, *J. Chem. Phys.* 93 (1990) 1061–1071.
[37] P.E. Blöchl, Projector augmented-wave method, *Phys. Rev. B* 50 (1994) 17953.
[38] S. Grimme, Semiempirical GGA-type density functional constructed with a long-range dispersion correction, *J. Comput. Chem.* 27 (2006) 1787–1799.
[39] J.P. Perdew, K. Burke, M. Ernzerhof, Generalized gradient approximation made simple, *Phys. Rev. Lett.* 77 (1996) 3865.
[40] S. Nosé, A molecular dynamics method for simulations in the canonical ensemble, *Mol. Phys.* 52 (1984) 255–268.